Research Article | Vol. 26, No. 15 | 23 Jul 2018 | OPTICS EXPRESS 19456
Optics EXPRESS

Optical design of a prism–grating-based lenslet array integral field spectrometer

JIANAN LIU,[1,2,3] JIANJUN CHEN,[1,2] JIANLI LIU,[1,2] SHULONG FENG,[1] XIAOTIAN LI,[1] AND JICHENG CUI[1,*]

[1]*Changchun Institute of Optics, Fine Mechanics and Physics, Chinese Academy of Sciences, Changchun Jilin 130033, China*
[2]*University of Chinese Academy of Science, Beijing 100049, China*
[3]*liu_jianan0926@163.com*
[*]*jicheng_cui@163.com*

Abstract: The optics for an integral field spectrometer based on a lenslet array is described. The principle behind the integral field spectroscopy of this system is introduced and partial modeling of the structure of the system is developed. A hybrid design method from physical optics and geometrical optics is used to design the system. Because the functions of the optical system before and after the lenslet array are different, the telephoto system and the spectrograph need to be separated. The optical system was then optimized using a combination design. This method is confirmed by simulation and comparison results and can be used in the design of other lenslet array integral field spectrometers.

1. Introduction

Since the 1980s, the imaging spectrometer has been developed for multi-spectral remote sensing technology [1]. Hyperspectral images of a scene or target can be obtained with high spectral resolution, and both target image information and spectral information can be obtained simultaneously. In its most basic scheme, with the observed sample illuminated by a broadband light source, the imaging spectrometer is a line-scanning hyperspectral imaging system [2–4]. Transmitted light, containing information of the observed sample, is collected using input optics, then passed through a narrow slit, and finally dispersed across the detector forming one spatial slice of hyperspectral image [5–8]. Because of limitation of the slit, we cannot get the complete information of the target with a single scan. Multiple scans are needed along the direction perpendicular to the slit to obtain a complete set of data; the scanning is time consuming.

The lenslet array integral field spectrometry (IFS) is a fast and efficient type of three-dimensional imaging spectrometer, initially used in astronomy [9-10]. The spectrometer obtains a spectrum of each spatial element in its fields-of-view, producing a cube of data corresponding to two spatial (x, y) and one spectral (λ) dimension [11]. It gathers complete information of the celestial body, greatly saving valuable observation time on the telescope, and improves the stability and consistency of the observed data. It has proved to become one of the most effective means for performing three-dimensional imaging spectroscopy and a central focus in present-day technological advances in astronomical instrumentation [12].

Among the diffraction limited and cryogenic IFS, the OSIRIS spectrometer of the Keck telescope was the first lenslet array IFS, designed and manufactured by the University of California. Successors, GPI and IRIS, were also based on the OSIRIS spectrometer and developed by the University of California. OSIRIS has a high spectral resolution and a large field-of-view (FOV), but less observable spectral channels. Compared with OSIRIS, GPI can acquire a higher number of observable spectra, but the spectral resolution is lower and the angle of view is smaller. IRIS improved on both OSIRIS and GPI in regard to spectral resolution and field angle; it far exceeds OSIRIS, but the number of acquired spectra is much lower than GPI although slightly higher than that of OSIRIS. In addition, CHARIS is a lenslet

#328558 https://doi.org/10.1364/OE.26.019456
Journal © 2018 Received 20 Apr 2018; revised 28 Jun 2018; accepted 4 Jul 2018; published 18 Jul 2018

Optics EXPRESS

array integrating field spectrometer developed by Princeton University. The spectroscopic element is a prism with both highand low spectral resolution modes. The dispersing component of GPI and CHARIS is a prism, whereas IRIS and OSIRIS have a grating [13–16].

We present an alternative optical design based on a prism-grating (PG) dispersion system for a lenslet array IFS. The PG system can correct curvature of the spectral lines and reduce post-calibration work and data processing difficulties [17]. The lenslet array replaces the slit of the traditional imaging spectrometer and samples the FOV. The lenslet array is located at the focal plane of the telephoto system. At the focus of each lenslet a much smaller pupil image is formed that contains all of the light from its portion of the field. This lenslet array serves to spatially sample the input image. The pupil images are well separated and serve to define the entrance aperture of the spectrograph section [18].

In the design of the optical system, parameter selection of the lenslet array is key to the system design. In this paper, a hybrid design method of physical optics and geometrical optics is used to build the structural model of the lenslet array. The telephoto system and the spectrograph are analyzed before the lenslet array. The whole system was optimized using combination design. Simulation and comparision results are also described in detail. This method can be used in the design of other lenslet array IFS.

2. Optical layout for the lenslet array IFS

The IFS based on a lenslet array (Fig. 1) consists of a telephoto system, an integral field unit, and a spectrograph [19]. The spectrograph is composed of a collimation system, a dispersion system, and a camera system. The lenslet array, which is located on the focal plane of the telephoto system, serves to spatially sample the input image, and then focuses the light onto a sparse grid. Light from each spatial element is then dispersed by a dispersion system before eventually landing on the detector. We then use thousands of mini-spectra to reconstruct the data cube corresponding to the *(x, y, λ)* dimensions, the spectra of each spatial element of the FOV. We can acquire all the data simultaneously in one exposure without scanning or the push-broom acquisition process, so that the information is obtained at the same time thus ensuring its stability.

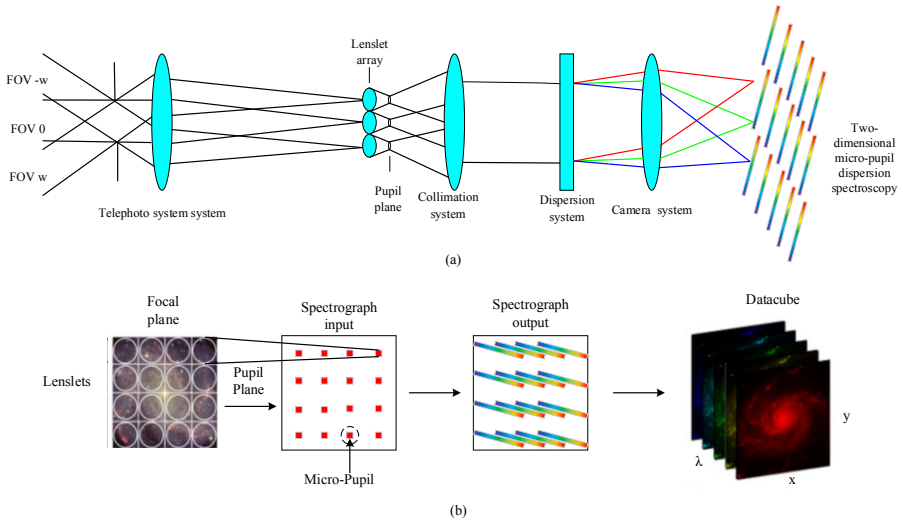

Fig. 1. Principle of the lenslet-array IFS.

Optics EXPRESS

3. Working principles of lenslet array IFS

3.1 Geometrical optical analysis of the lenslet array

To ensure the appropriate propagation of rays to from the lenslet array, there are some boundary conditions that need considering in regard to the angular relationship between the telephoto system and the lenslet array. The FOV of the telephoto system is denoted by *2w* (Fig. 1), and its focal length by *f'* (Fig. 2). The angle of incidence of light with the lenslet array is denoted by w_n. The lenslet has size *p*, thickness *T* and focal length *f*. The refractive index of the lenslet array is denoted by *n*. The diameter of the micro-pupil is φ. *R* is the radius of curvature of the lenslet. According to the principle of geometrical optics, we have:

$$\begin{cases} \sin\theta = \dfrac{p}{2R} \\ \alpha = i + \dfrac{w_n}{2} \end{cases}. \tag{1}$$

When light is incident on the front surface of the lenslet array, according to Snell's law of light refraction, we have:

$$\sin i = n \sin i'. \tag{2}$$

From the theorem of the exterior angle of a triangle, we obtain:

$$i' + i'' = \theta. \tag{3}$$

For the light incident on the second surface of the lenslet array, Snell's law of refraction gives

$$\begin{cases} n \sin i'' = \sin i''' \\ n \sin \alpha'' = \sin \alpha''' \end{cases}. \tag{4}$$

Furthermore, from geometrical optics, we can get Eqs. (5), (6), (7):

$$h_1 = f \tan i'''. \tag{5}$$

$$h_2 = f \tan \alpha'''. \tag{6}$$

$$h_3 = t(\tan i'' - \tan \alpha''). \tag{7}$$

The principle of vector height, to give Eq. (8)

$$t = T - \frac{p}{2} \tan[\arcsin(\frac{p}{2R})]. \tag{8}$$

And that the expression of the diameter of the micro pupil φ is:

$$\begin{aligned} \varphi / 2 &= h_1 - h_2 + h_3. \\ &= 2f \tan\{\arcsin[n \cdot \sin(\theta - \arcsin\frac{\sin i}{n})]\} - 2f \tan\{\arcsin[n \cdot \sin(\theta - \arcsin\frac{\sin(i + \frac{w_n}{2})}{n})]\} \\ &+ 2t \tan(\theta - \arcsin\frac{\sin i}{n}) - 2t \tan\theta - \arcsin\frac{\sin(i + \frac{w_n}{2})}{n}) \end{aligned}. \tag{9}$$

Substituting Eqs. (5), (6), (7) and (8) into Eq. (9), the expression of micro pupil diameter φ can be obtained.

Optics EXPRESS

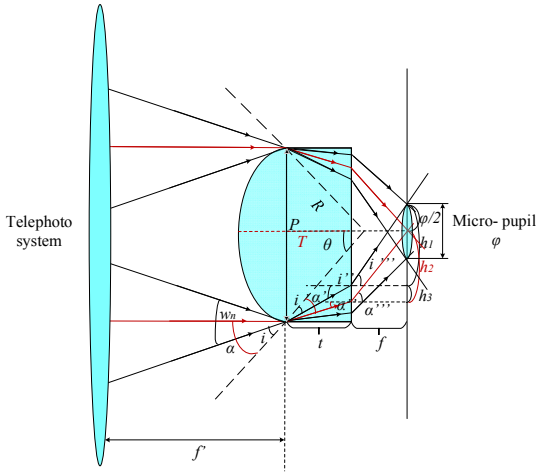

Fig. 2. Schematic of the micro-pupil.

3.2 Limit of the telephoto system

On-axis, the field angle corresponding to n-th lenses in lenslet array is $\theta_n/2$. To obtain pure information with no crosstalk and equal phase, there is also a limit on the chief ray in the different fields of view, specifically, the telecentricity of the telephoto system. The telephoto system has coma, spherical aberration. The main cause of coma aberration is that the off-axis object point is out of symmetry after being imaged by the optical system, so it will affect the angle that the chief ray incident on the plane of the lenslet array, and lead to a chief ray of each field out of the perpendicular to the lenslet array plane. Let α denote the incident angle of the chief ray of the n-th field to the lenslet array plane, and ω the position angle of each lenslet. When α exceeds $\omega/2$, the image that should be on the n-th lenslet is on the (n-1)-th lenslet, and this leads to crosstalk in the acquired information. Crosstalk causes great error in data processing. In summary, the telecentricity of the telephoto system, α should satisfy the incident angle condition:

$$\alpha \le \frac{\theta_n}{2}. \tag{10}$$

The target objects are imaged on the lenslet array by the telephoto system. To ensure that each lenslet can obtain a clear image, a limit is imposed on the FOV of the telephoto system. Let the diagonal length of the lenslet array be denoted h and the FOV of the telephoto system be denoted $2w$, and the angular magnification of the telephoto system is γ. Hence, the value of the lower limit of the angle $2w$ is chosen as:

$$2w = 2\arctan(\frac{h}{2f'})/\gamma. \tag{11}$$

3.3 Physical optics analysis and the simulation of the lenslet array

To analyze diffraction at the micro-pupil plane, an approximation of Fresnel diffraction is necessary [20]. For Fresnel diffraction, the complex amplitude distribution of the sample plane is:

Optics EXPRESS

$$\tilde{E}(x,y)=\frac{\exp(ikz)}{i\lambda z}\exp(ik\frac{x^2+y^2}{2z})\int\int_{-\infty}^{+\infty}\tilde{E}_0(x_1,y_1)\times\exp\left[\frac{ik}{2z}(x_1^2+y_1^2)\right]\times\exp\left[-i\frac{2\pi}{\lambda z}(xx_1^2+yy_1^2)\right]dx_1dy_1. \tag{12}$$

Where λ is the wavelength, x and y are the coordinates in the sample plane, x_1 and y_1 are the coordinates in the diffraction screen (here is the lenslet array rear plane), and z is the distance between the sample plane and the diffraction screen; $exp(ikz_1)/i\lambda z_1$ is an amplitude with wave number $k = 2\pi\sigma$ and phase factor independent of x_1, y_1. If the width of the diffraction screen is much smaller than z, when z shifts around a little from a reference distance z_0, only the factor $exp(ikz)$ in Eq. (12) changes. Equation (12) can be rewritten as

$$\tilde{E}(x,y)=\frac{\exp(ikz_1)}{i\lambda z_1}\int\int_{-\infty}^{+\infty}\tilde{E}(x_1,y_1)\exp\left\{\frac{ik}{2z_1}\left[(x-x_1)^2+(y-y_1)^2\right]\right\}dx_1dy_1. \tag{13}$$

The definition of the complex amplitude is written as:

$$\tilde{E}(x_1,y_1)=\tilde{E}_0(x_1,y_1)\tilde{t}(x_1,y_1). \tag{14}$$

Where $t(x_1y_1)$ is the transmittance function. The lens always has a certain aperture size and that limits the wave surface, resulting in diffraction effects. To show these limited aperture effects of the lens, a pupil function can be introduced to represent the finite aperture of the lens. The complex amplitude of the lens transmittance can be expressed as:

$$\tilde{t}(x_1,y_1)=P(x_1,y_1)\exp\left(-ik\frac{x_1^2+y_1^2}{2f}\right). \tag{15}$$

Where $P(x_1,y_1)$ is the pupil function. Recall that the lenslet array is on the focal plane of the telephoto system on which is the telecentric structure. If we consider a single rectangular lens, then according to the Fourier transform properties of the lens, the pupil function is expressed as:

$$P(x_1,y_1)=rect(\frac{x_1}{a})rect(\frac{y_1}{b})=\begin{Bmatrix}a & |x_1|\le\frac{a}{2} & |y_1|\le\frac{b}{2}\\ 0 & others\end{Bmatrix}. \tag{16}$$

Where a and b are the length and width of the lenslet respectively, and $rect(x_1/a)rect(y_1/b)$ is the rectangular aperture function. We assume the transmittance of the lens is $t_0(x_1,y_1)$, and its frequency spectrum is $T_0(f_x,f_y)$. The diffraction screen has a lens of exactly the same shape as that above. The orientation of these apertures is exactly the same, implying that each lens can be translated by any other aperture. If a point corresponding to a position in each lens is used to represent the position of the lens, the transmittance function of the entire diffraction screen can be expressed as a linear combination of single lens transmittances:

$$t(x_1,y_1)=\sum_{n=1}^{N}t_0(x_1-\xi_n,y_1-\eta_n). \tag{17}$$

Using the screening properties of the δ function, the above equation can be rewritten as:

$$t(x_1,y_1)=t_0(x_1,y_1)*\sum_{n=1}^{N}\delta(x_1-\xi_n,y_1-\eta_n). \tag{18}$$

Optics EXPRESS

This means the transmittance of the whole function is a convolution of two functions, for which the transmittance of each single lens is described as $t(x_1,y_1)$, and the position of each δ function in the two-dimensional array of δ functions represents the position of each single lens. The transmittance function can be expressed as:

$$t(x_1,y_1)=P(x_1,y_1)\exp\left(-ik\frac{x_1^2+y_1^2}{2f}\right)*\sum_{n=1}^{N}\delta(x_1-\xi_n,y_1-\eta_n) \tag{19}$$

As the lenslet array is located at the focal plane of the telephoto system, which is the telecentric structure in the image space, according to the Fourier transform properties of the lens, and neglecting the influence of aberration, the incident wave can be approximated as a plane wave. First, in regard to the monochromatic wave, the complex amplitude distribution of the incident wave is simply $E_0(x,y) = 1$. Then, substituting the complex amplitude distribution of the incident wave and the transmittance function into Eq. (12), we can get the amplitude expression. Equation (13) can be written as:

$$\begin{aligned}\tilde{E}(x,y)=\frac{\exp(ikz_1)}{i\lambda z_1}\int_{-\infty}^{+\infty}\int\left[rect(\frac{x_1}{a})rect(\frac{y_1}{b})\exp\left(-ik\frac{x_1^2+y_1^2}{2f}\right)\right]*.\\ \sum_{n=1}^{N}\delta(x_1-\xi_n,y_1-\eta_n)\exp\left\{\frac{ik}{2z_1}\left[(x-x_1)^2+(y-y_1)^2\right]\right\}dx_1dy_1.\end{aligned} \tag{20}$$

For a continuous light source, as the interferogram is only the overlap of interferograms of different wavelengths, the discussion above is still valid. With the above theoretical analysis, a mathematical calculation model was configured, and the optical design model was established for verification. Under the same size of a rectangular on-axis lenslet, the Physical Optics Propagation of the Optical design software predicts the same encircled energy. Figure 3 shows the amplitude and light intensity at the focal plane behind the lenslet array; Fig. 4 shows the micro-pupil model in mathematical calculation software and optical design software, respectively. For the mathematical calculation model and optical design model with the same parameter setting, the resulting micro-pupils have the same size implying the mathematical calculation model is consistent with the actual micro-pupil model.

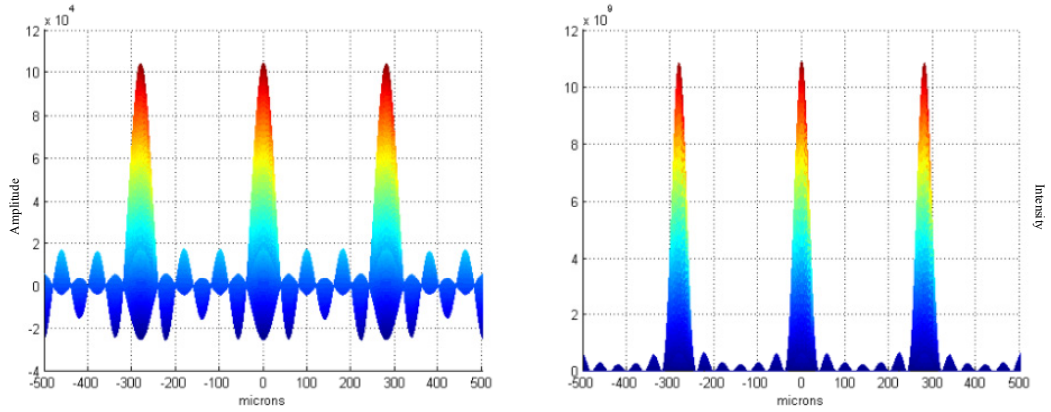

Fig. 3. Simulation of amplitude (left) and light intensity (right) at the focal plane behind the lenslet array. Size of the lenslet p is 280μm, and $F/\#$ is 4.

Optics EXPRESS

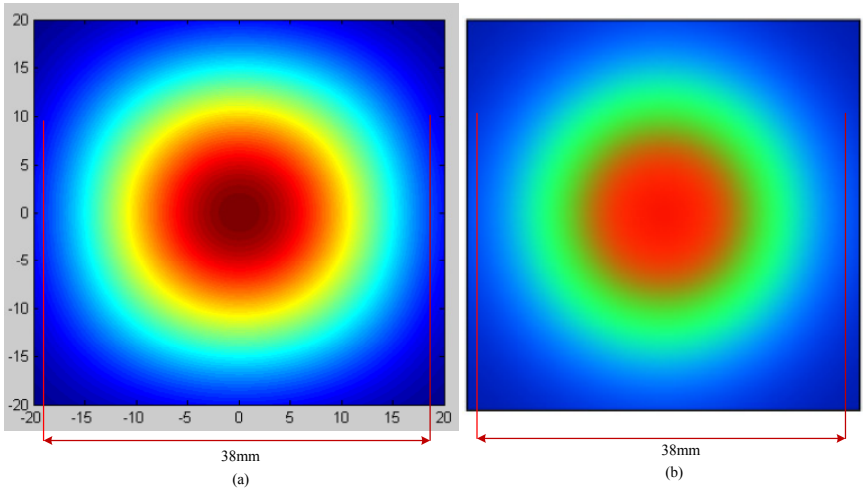

Fig. 4. Simulation of the micro-pupil intensity using the mathematical calculation software (left) and the optical design software (right). The input parameters of the lenslet array are the same: $p = 280\mu m$, $F/\# = 4$. And the results are the same.

Based on our mathematical calculation model, an analysis of the micro-aperture energy and crosstalk for different *F/#* was simulated. Figure 5 shows the energy distribution of the micro-pupil at different focal lengths of the lenslet array.

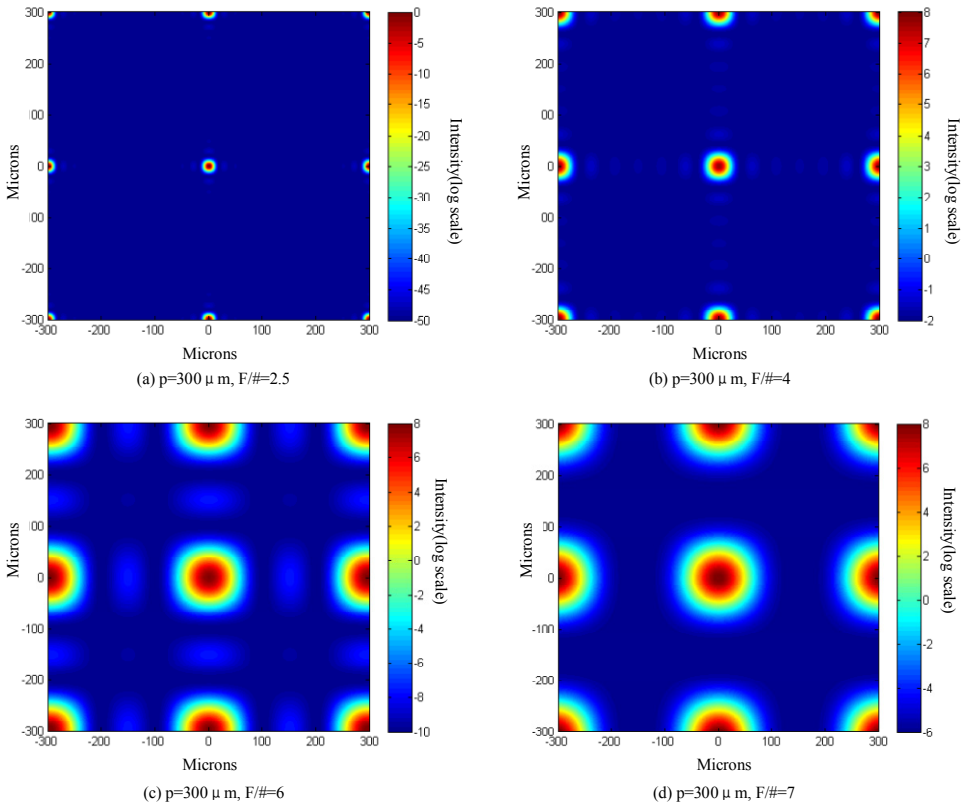

Fig. 5. Different *F/#* of the lenslet at fixed diameter. When we fix the size of the lenslet and decrease the *F/#* of the lenslet, the lenslet crosstalk increases.

Optics EXPRESS

Figure 6 shows the micro-pupil size and crosstalk under different sizes of lenslet. From the simulation results, when increasing the micro-pupil separation by increasing the pitch while holding the lenslet *f*-number fixed, the lenslet crosstalk decreases. Faster *f*-number lenslets have a smaller diffraction pattern (and hence, less crosstalk).

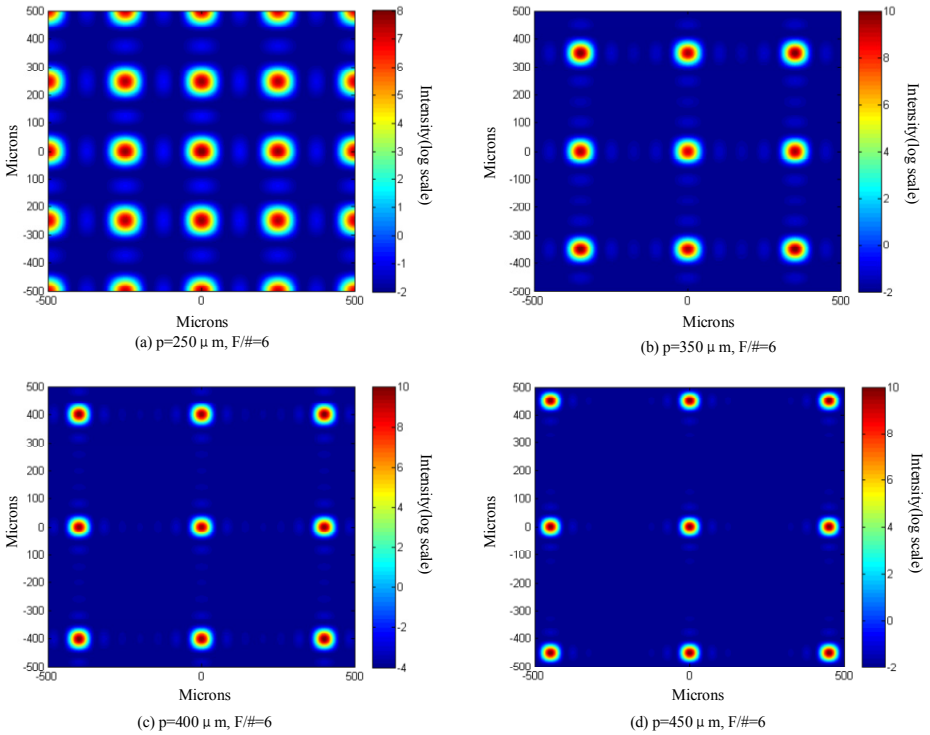

Fig. 6. Simulation of the crosstalk for different diameters of the lenslet at fixed *F/#*. From the simulation results, when increasing the micro-pupil separation by increasing the pitch while holding the lenslet *f*-number fixed, the lenslet crosstalk decreases.

3.4 Spectrograph pupil-matching system analysis

To match with the telephoto system and the lenslet array pupil, the numerical aperture should be larger than $2i'''$ of that shown in Fig. 2 when designing the camera system, with i''' obtained from:

$$i''' = \arctan\left(\frac{\phi}{2f}\right). \tag{21}$$

The aperture angle from the micro-pupil exit to the camera system, denoted u (Fig. 7), equals the object-side aperture angle of the spectrograph (i.e., $u = i''$).

Optics EXPRESS

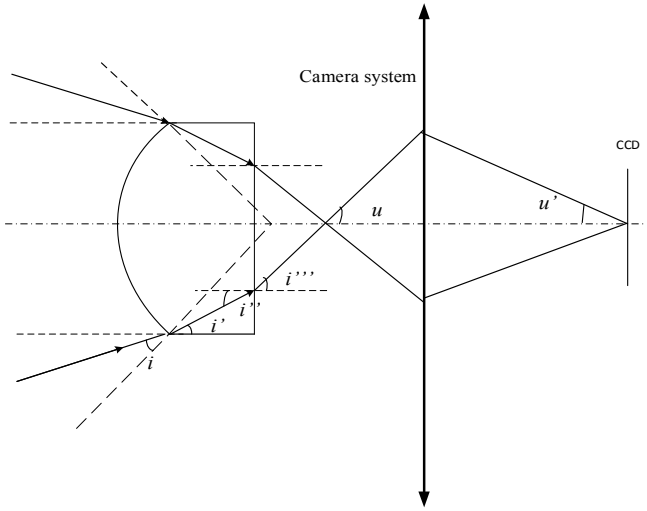

Fig. 7. Pupil matching of the lenslet array and the spectrograph.

In the direction of dispersion of the CCD, the lenslet array is of size p, with an array number $x \times y$ (x is the dispersion direction). Let the pixel size of CCD be denoted by q; the magnification of the camera system is given by:

$$m = hq / xp. \tag{22}$$

The exit angle of the light ray through the camera system is u', and from the magnification, we find the image-side aperture angle of the rear system to be:

$$u' = u / m. \tag{23}$$

4. Design of systems

In order to reduce the aberration caused by refraction lenses, especially the color aberration, we select off-axis three-mirror anastigmatic (TMA) system as telephoto system. The incident angle of the chief ray of each FOV at the image plane is less than one-half of the FOV corresponding to each array lens. The range of wavelengths is 400–800 nm; the half-FOV angle is 2°, whereas the main FOV of the incident angle is less than 0.2°. The primary mirror, the secondary mirror, and the third mirror of the TMA all have a secondary aspherical surface to eliminate the high aberration of the system and reduce the number of mirrors of the system. One more mirror was added to the three mirrors to fold the optical path to create a system of smaller size [21–23].

The spectrograph system includes a collimation system, a dispersion system, and a camera system. The dispersion system is the combined PG system. The dispersion spectra of the prism and the grating oppose each other, so their combination is conducive to correcting curvature of the spectral lines. The function of the spectrometer system is to collimate the light exiting the lenslet array, then to disperse the light, and finally to image it on the detector. The collimation system and camera system are double Gaussian symmetry structure, which are more conducive to aberration correction. Both these systems use spherical lenses. The input field size and f-number must match that of the lenslet array. In Table1 we list the system requirements for the spectrograph system. Figures 8, 9, 10, and 11 present a schematic of the optical path, modulation transfer function (MTF), spot, and aberration curves of the spectrograph. The optical path and the resolution of the IFS system are presented in Figs. 12 and 13, respectively.

Optics EXPRESS

Table 1. Specifications of the spectrograph system

Parameter	Value
Spectral range/nm	400-800
Field of view/mm	± 7
F number	2.4
Spectral resolution /nm	≤1
Detector pixel size /μm	7.4 × 7.4
Detector array size/mm	14 × 7

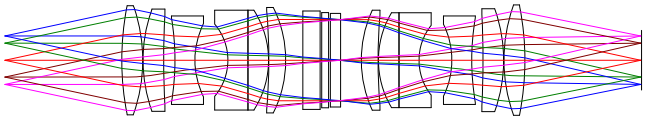

Fig. 8. Optical path of the spectrograph.

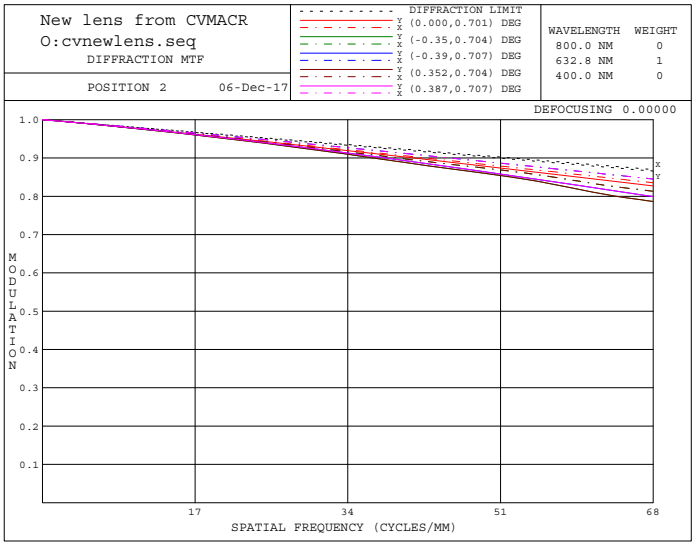

Fig. 9. Modulation transfer function of the spectrograph.

Optics EXPRESS

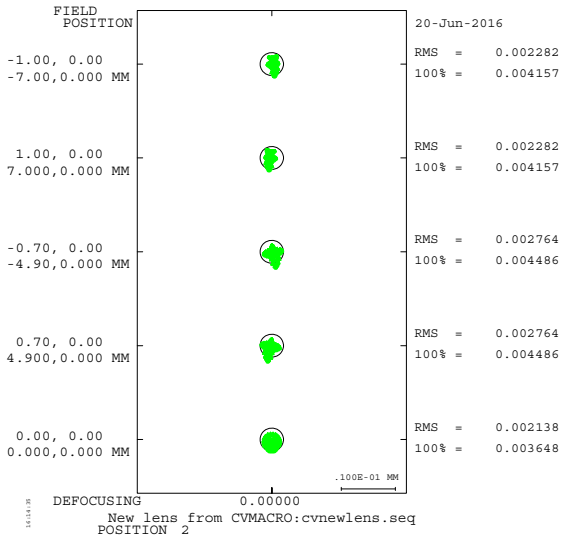

Fig. 10. Spot of the spectrograph.

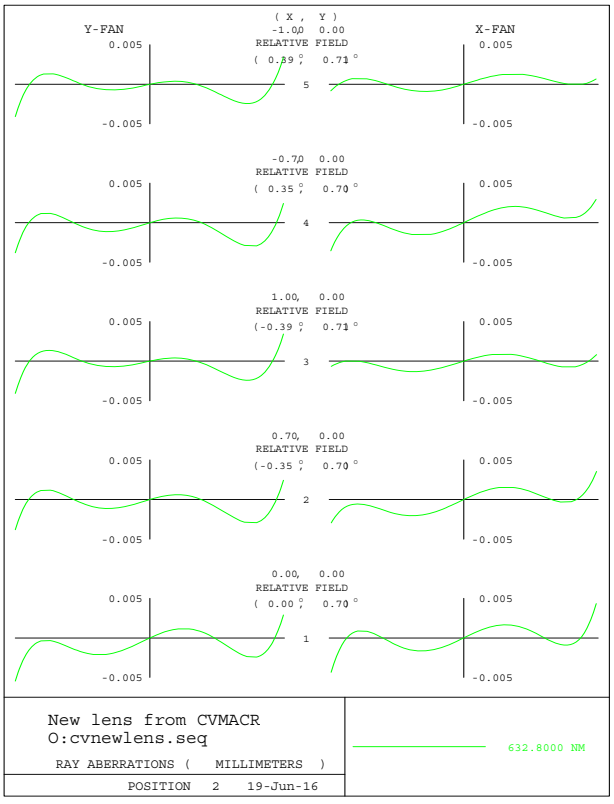

Fig. 11. Aberration curve of the spectrograph.

Optics EXPRESS

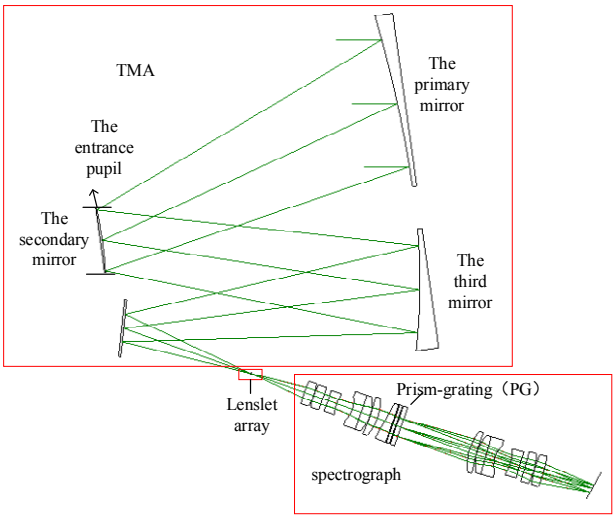

Fig. 12. Optical design of the IFS system.

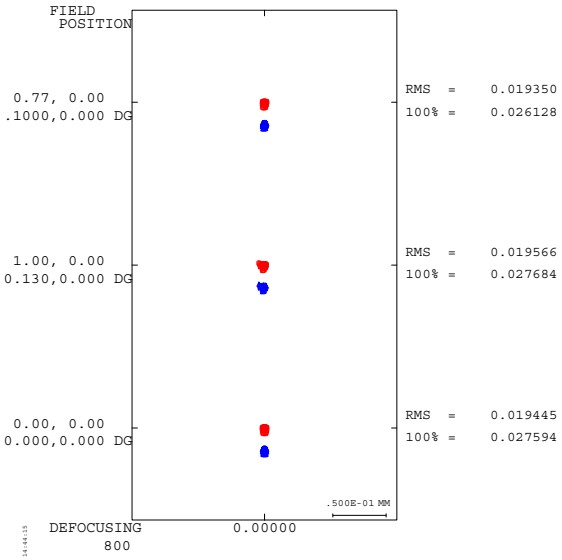

Fig. 13. Resolution of the IFS system.

For different parameters of the lenslet array, the spot diagram and the resolution obtained by the system are very different. According to the analysis of section 3.3, the parameters of the lenslet array with large crosstalk of micro pupil energy and the parameters of the lenslet array with small crosstalk are introduced into the CODE V optical design software. Three sets of spot diagrams are obtained, as shown in Fig. 14, and the parameters of the three lenslet arrays is in Table 2. The wavelengths in the graphs in Fig. 14(a) and 14(b) are both 800nm and 799nm, and the wavelengths in Fig. 14(c) are 800nm and 798nm. It can be seen from the (a) and (b), spot diagrams that the spectrum of 800nm and 799nm can be clearly distinguished, and the spectral resolution is 1nm; 800nm and 798nm can be clearly distinguished in the Fig. 14(c), and the spectral resolution is 2nm. For different lenslet parameters, the final spot and spectral resolution obtained on the detector will be very different. Use the established model to analyze the optimized micro pupil, substituting the parameters of the lenslet array with small crosstalk into the software, the resulting spot and spectral resolution are better. In contrast, substituting the parameters with more crosstalk, we get poor spot and lower spectral resolution.

Optics EXPRESS

Table 2. Parameters for Fig. 14

	Figure 14(a)	Figure 14(b)	Figure 14(c)
ROC	0.625mm	0.715mm	0.625mm
Thickness	1.0mm	1.2mm	1.3mm
Resolution	<1nm	1nm	2nm

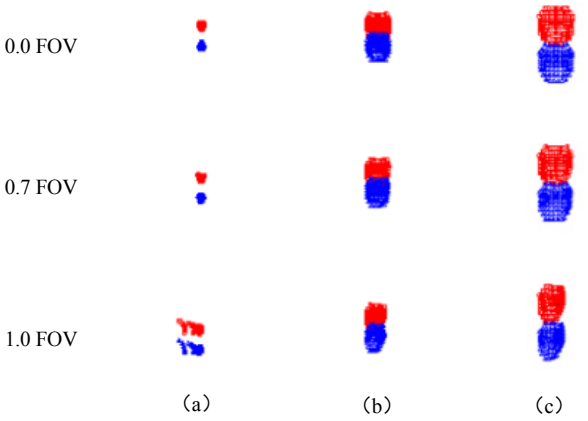

Fig. 14. Spot diagram under different lenslet parameters.

5. Conclusions

An integrated FOV imaging spectrometer structure based on lenslet array has been described along with its working principle. The micro-pupil diameter of the lenslet array IFS was analyzed, and a specific expression of its size obtained. From the way the micro-pupil functions, the range of incident angle and the range of the fields of view of the telephoto system were obtained by analyzing the incident angle of the main ray and the image plane of each FOV. To reduce crosstalk of the spectral images obtained at the detector, the functioning of the micro-pupil was evaluated and simulated. The different lenslet array parameters were brought into the optical design software for overall simulation.

We systematically summarized the design methods of the lenslet array IFS and elaborated the complete set of design methods in detail and completed. As a verification of the method in the text, we used this method to design the actual system, and finally obtained satisfactory design results. This article provides a set of complete and feasible design methods, which can provide guidance and reference for the design of related optical systems.

Funding

Chinese Finance Ministry for the National R&D Projects for Key Scientific Instruments (Grant No. ZDYZ2008-1); National Natural Science Foundation of China (Grant No. 61505204); from Ministry of National Science and Technology for National Key Basic Research Program of China (Grant No. 2014CB049500); National Key Scientific Instrument and Equipment Development Projects in China (Grant No. 2014YQ120351); Jilin Outstanding Youth Project in China (Grant No. 20170520167JH).

References

1. J. Reimers, A. Bauer, K. P. Thompson, and J. P. Rolland, "Freeform spectrometer enabling increased compactness," Light Sci. Appl. **6**(7 e17036), e17026 (2017).

Optics EXPRESS

2. M. Kosec, M. Bürmen, D. Tomaževič, F. Pernuš, and B. Likar, "Characterization of a spectrograph based hyperspectral imaging system," Opt. Express **21**(10), 12085–12099 (2013).
3. Z. Zhang, B. Hu, Q. Yin, T. Yu, S. Li, X. Gao, and H. Zhang, "Design of short wave infrared imaging spectrometer system based on CDP," Opt. Express **23**(23), 29758–29763 (2015).
4. P. Cu-Nguyen, A. Grewe, P. Feßer, A. Seifert, S. Sinzinger, and H. Zappe, "An imaging spectrometer employing tunable hyperchromatic micro lenses," Light Sci. Appl. **5**(4 e16058), e16058 (2016).
5. R. M. Sullenberger, A. B. Milstein, Y. Rachlin, S. Kaushik, and C. M. Wynn, "Computational reconfigurable imaging spectrometer," Opt. Express **25**(25), 31960–31969 (2017).
6. J. W. Pan, C. M. Wang, H. C. Lan, W. S. Sun, and J. Y. Chang, "Homogenized LED-illumination using microlens arrays for a pocket-sized projector," Opt. Express **15**(17), 10483–10491 (2007).
7. L. Yuan, Z. He, G. Lv, Y. Wang, C. Li, J. Xie, and J. Wang, "Optical design, laboratory test, and calibration of airborne long wave infrared imaging spectrometer," Opt. Express **25**(19), 22440–22454 (2017).
8. L. Yu, "Upgrade of a UV-VIS-NIR imaging spectrometer for the coastal ocean observation: concept, design, fabrication, and test of prototype," Opt. Express **25**(13), 15526–15538 (2017).
9. J. L. Rasilla, R. L. López, C. Tejada, "OSIRIS Optical integration and tests," Proc. SPIE **7014**, 701438 (2008).
10. M. McElwain, J. Larkin, S. Metchev, and B. Zuckerman, "High-Contrast Imaging with Keck Adaptive Optics and OSIRIS," Proc. SPIE **7015**, 70151A (2008).
11. S. Thibault, P. Vallée, E. Artigau, J. Maire, R. Doyon, J.-F. Lavigne, and J. Larkin, "GPI – Cryogenic Spectrograph Optics Performances," Proc. SPIE **7735**, 77351N (2010).
12. J. E. Larkin, "Diffraction Limited Integral Field Spectrographs for Large Telescopes," Proc. SPIE **9192**, 91920C (2014).
13. S. Thibault, "Cryogenic Lens Design Case Study: Gemini Planet Imager Spectrograph," Proc. SPIE **8128**, 812802 (2011).
14. J. E. Larkin, A. Quirrenbach, A. Krabbe, T. Aliado, M. Barczys, G. Brims, J. Canfield, T. Gasaway, D. L. Freniere, N. Magnone, G. Skulason, M. Spencer, D. Sprayberry, and J. Weiss, "OSIRIS, An Infrared Integral Field Spectrograph for the Keck Adaptive Optics System," Proc. SPIE **4841**, 1600–1610 (2003).
15. J. Larkin, M. Barczys, A. Krabbe, S. Adkins, T. Aliado, and P. Amico, "OSIRIS: A Diffraction Limited Integral Field Spectrograph for Keck," Proc. SPIE **6269**, 62691A (2006).
16. A. Krabbe, J. E. Larkin, C. Iserlohe, M. Barczys, A. Quirrenbach, M. McElwain, J. Weiss, and S. A. Wright, "First results with OSIRIS: NIR-imaging spectroscopy at the diffraction limit," Proc. SPIE **6269**, 62694Q (2006).
17. Z. Yang, Y. Tang, M. Bayanheshig, J. Cui, J. Yang, "Optimization Design Method for Optical System of Prism-Grating Ultraspectral Imaging Spectrometers," Acta Optica Sinica **34**, 0911003 (2014).
18. L. Chen, S. Kirchberg, B. Y. Jiang, L. Xie, Y. L. Jia, and L. L. Sun, "Fabrication of long-focal-length plano-convex microlens array by combining the micro-milling and injection molding processes," Appl. Opt. **53**(31), 7369–7380 (2014).
19. D. Lee, R. Haynes, D. Ren, and J. Allington-Smith, "Characterization of Lenslet Arrays for Astronomical Spectroscopy," PASP **113**(789), 1406–1419 (2001).
20. C. Feng, B. Wang, Z. Liang, and J. Liang, "Miniaturization of step mirrors in a static Fourier transform spectrometer: theory and simulation," J. Opt. Soc. Am. B **28**(1), 128–133 (2011).
21. J. Cui, Y. Tang, P. Han, M. Pan, and J. Zhang, "Development of diagnostic imaging spectrometer for tumor on-line operation," Optics and Precision Engineering **21**(12), 3043–3049 (2013).
22. C. Yan, J. Xu, and Y. Peng, "Stray light suppression of three-mirror off-axis space optical telescope," Optics and Precision Engineering **18**(2), 290–293 (2010).
23. Q. Xue, "Design of wide field of view off-axis three-mirror system for hyperspectral imager," Hongwai Yu Jiguang Gongcheng **41**(4), 943–946 (2012).